Spectroscopy, morphometry, and photoclinometry of Titan's dunefields from Cassini/VIMS

Jason Barnes, Robert Brown, Laurence Soderblom, Christophe Sotin, Stéphane Le Mouélic, Sebastien Rodriguez, Ralf Jaumann, Ross Beyer, Bonnie Buratti, Karly Pitman, et al.

Available online at www.sciencedirect.com
ScienceDirect
Icarus 195 (2008) 400–414
ICARUS
www.elsevier.com/locate/icarus

Spectroscopy, morphometry, and photoclinometry of Titan's dunefields from Cassini/VIMS

Jason W. Barnes [a,*], Robert H. Brown [b], Laurence Soderblom [c], Christophe Sotin [d], Stèphane Le Mouèlic [e], Sebastien Rodriguez [f], Ralf Jaumann [g], Ross A. Beyer [a], Bonnie J. Buratti [d], Karly Pitman [d], Kevin H. Baines [d], Roger Clark [h], Phil Nicholson [i]

[a] *NASA Ames Research Center, M/S 244-30, Moffett Field, CA 94035, USA*
[b] *Department of Planetary Sciences, University of Arizona, Tucson, AZ 85721, USA*
[c] *United States Geological Survey, Flagstaff, AZ 85001, USA*
[d] *Jet Propulsion Laboratory, Caltech, 4800 Oak Grove Drive, Pasadena, CA 91109, USA*
[e] *Universite de Nantes, Laboratoire de Planetologie et Geodynamique, 2 rue Houssinere, 44322 Nantes Cedex 03, France*
[f] *Laboratoire AIM, Centre d'ètude de Saclay, DAPNIA/Sap, Centre de l'Orme des Merisiers, bât. 709, 91191 Gif/Yvette Cedex, France*
[g] *DLR, Institute of Planetary Research, Rutherfordstrasse 2, D-12489 Berlin, Germany*
[h] *United States Geological Survey, Denver, CO 80225, USA*
[i] *Department of Astronomy, Cornell University, Ithaca, NY 14853, USA*

Received 5 October 2007; revised 9 December 2007

Available online 3 January 2008

Abstract

Fine-resolution (500 m/pixel) *Cassini* Visual and Infrared Mapping Spectrometer (VIMS) T20 observations of Titan resolve that moon's sand dunes. The spectral variability in some dune regions shows that there are sand-free interdune areas, wherein VIMS spectra reveal the exposed dune substrate. The interdunes from T20 are, variously, materials that correspond to the equatorial bright, 5-μm-bright, and dark blue spectral units. Our observations show that an enigmatic "dark red" spectral unit seen in T5 in fact represents a macroscopic mixture with 5-μm-bright material and dunes as its spectral endmembers. Looking more broadly, similar mixtures of varying amounts of dune and interdune units of varying composition can explain the spectral and albedo variability within the dark brown dune global spectral unit that is associated with dunes. The presence of interdunes indicates that Titan's dunefields are both mature and recently active. The spectrum of the dune endmember reveals the sand to be composed of less water ice than the rest of Titan; various organics are consistent with the dunes' measured reflectivity. We measure a mean dune spacing of 2.1 km, and find that the dunes are oriented on the average in an east–west direction, but angling up to 10° from parallel to the equator in specific cases. Where no interdunes are present, we determine the height of one set of dunes photoclinometrically to be between 30 and 70 m. These results pave the way for future exploration and interpretation of Titan's sand dunes.

Keywords: Titan; Geological processes; Satellites, atmospheres; Spectroscopy

1. Introduction

Contrary to prior theoretical prediction (Lorenz et al., 1995), *Cassini* found sand dunes on Titan (Lorenz et al., 2006). They are longitudinal dunes, which form parallel to the average wind direction and in wind regimes characterized by at least two different principal wind directions (Tsoar, 1983; Rubin and Ikeda, 1990; Lancaster, 1995). The areas covered by dunes are discernible in near-infrared spectral mapping by low albedo and a shallow red slope relative to the rest of Titan ("dark brown"; Soderblom et al., 2007). Global mapping shows that this dune-containing dark brown spectral unit covers a substantial fraction of Titan's surface at latitudes within 30° of the equator (Barnes et al., 2007a).

In this paper, we use observations from *Cassini*'s Visual and Infrared Mapping Spectrometer (VIMS; Brown et al., 2004)

* Corresponding author.
E-mail address: jason@barnesos.net (J.W. Barnes).

0019-1035/$ – see front matter
doi:10.1016/j.icarus.2007.12.006

Table 1
Summary of observations

Flyby	Date	Cube(s)	Geometry	Exp. time	Max res.	Solar zenith angle
Ta	2004 October 26	1477496141_1	64 × 64	80 ms	1.7 km	34°
T4	2005 March 31	1490990831_4	64 × 64	80 ms	1.2 km	45°
T20	2006 October 25	1540484750_1	$n = 910$			41°
		through		13 ms	485 m	
		1540484998_1	12 × 1			
T34	2007 July 19	1563501939_1	$n = 64$			42°
		through		50 ms	2.7 km	
		1563502438_1	1 × 64			

to investigate the nature of Titan's dunefields. We first describe the observations, which involve a novel mode of data acquisition. Next we investigate the morphology and spectral variability of the dunefields, revealing the existence of sand-free interdunes in some areas. We acquire and analyze spectra of both the dunes and interdunes to constrain composition. Next we measure dune spacings and orientations and determine the dunes' heights using photoclinometry before concluding.

2. Data reduction

The data that we analyze in this paper consist of VIMS observations from the Ta (2004 October 26), T4 (2005 April 31), T20 (2006 October 25), and T34 (2007 July 19) *Cassini* flybys of Titan. We show a summary of the data that we use in Table 1.

The Ta and T4 cubes are conventional cubes, 64 × 64 in spatial dimensions. The infrared half of VIMS is a spot-scanning instrument; it has a single, linear 256-element array that takes but a single spectrum at a time. To build up two-dimensional images it uses an actuated mirror that sweeps left-to-right (the 'x' or 'sample' dimension) before angling down by a single pixel (the 'y' or 'line' dimension), flying back like a typewriter, and starting a new left-to-right sweep. At the end of every line, the instrument takes a measurement of the background. We reduced them using the VIMS pipeline, as detailed in Barnes et al. (2007a): background subtraction, despike/desaturation, flat-field, conversion to I/F, and geometric projection.

The T20 and T34 observations were designed using a new and different mode of data acquisition. When VIMS observes near low-altitude closest approaches to Titan (within 2500 km or so), the spacecraft cannot turn quickly enough to stay pointed at a target on the moon's surface. In this case, we do not take full cubes as outlined above. Instead, we program the instrument to take repeated single-line cubes, moving the mirror only in the sample dimension, and rely on the spacecraft's motion relative to the moon's surface to build up the second spatial dimension. This results in many tens or hundreds of data cubes with spatial dimensions of N by 1. The exposure time and number of spectra N that we take in the sample dimension is determined by the requirement that the spacecraft have moved 1 pixel downtrack in the time that it takes VIMS to complete each line scan. For low-periapsis closest approaches like that on T20, this limits the width of the swath to 12 pixels near closest approach using the minimum necessary exposure time to achieve a signal-to-noise ratio of 100 in the 2 μm band (13 ms).

The resulting hundreds of 12 by 1 cubes that are the result of this observation mode, which we call "noodle mode" based on the aspect ratio of the geometrically projected result, must be reduced somewhat differently from cubes in "normal mode." If each of these 12 × 1s is reduced individually, then the resulting geometric projection shows striping in the sample dimension with an intensity comparable to that of the surface reflectivity. The striping is caused by the on-board background subtraction. With 13 ms exposures and no averaging between lines, the background measurement for each cube is tremendously noisy. Thus to defeat this noise we stitch the 12 × 1s into a single cube 12 by *nn* in size where *nn* is the number of 12 × 1 cubes in the observation. We re-add the on-board-subtracted background, and then subtract off the median background value for the entire *nn* cube sequence instead of the individual backgrounds being subtracted off of each 12 × 1 cube. We then complete the reduction in the same way as for normal mode cubes.

3. Spectral mapping

3.1. The dunes

Cassini's RADAR instrument sees dunes exclusively within the VIMS dark brown spectral unit (Soderblom et al., 2007). Soderblom et al. (2007) hypothesized that this dark brown endmember, and by extension the sand (defined as particles between 0.0625 and 2 mm in diameter) that makes up the dunes themselves, could be composed of complex hydrocarbons and/or nitriles. As the VIMS T20 swath passes through dark brown northern Fensal (see Fig. 1) with spatial resolution sufficient to resolve individual dunes (∼500 m/pixel), we use it to investigate the spectral characteristics of the sand dunes when we can see that they fill entire pixels.

The entire 12-pixel-wide portion of the T20 swath is shown in color in Fig. 2. As the swath extends over 900 pixels in the downrange dimension but is 12 pixels across, for this figure we rotated the cylindrically-mapped swath through Euler angles appropriate to straighten it out, and then compressed it in the downrange dimension in order to facilitate spectral comparisons within the swath. The combination of rotation and compression result in the unconventional latitude/longitude grid that surrounds the swath in Fig. 2 and introduces spatial distortions to the resulting image. For interpreting morphology and

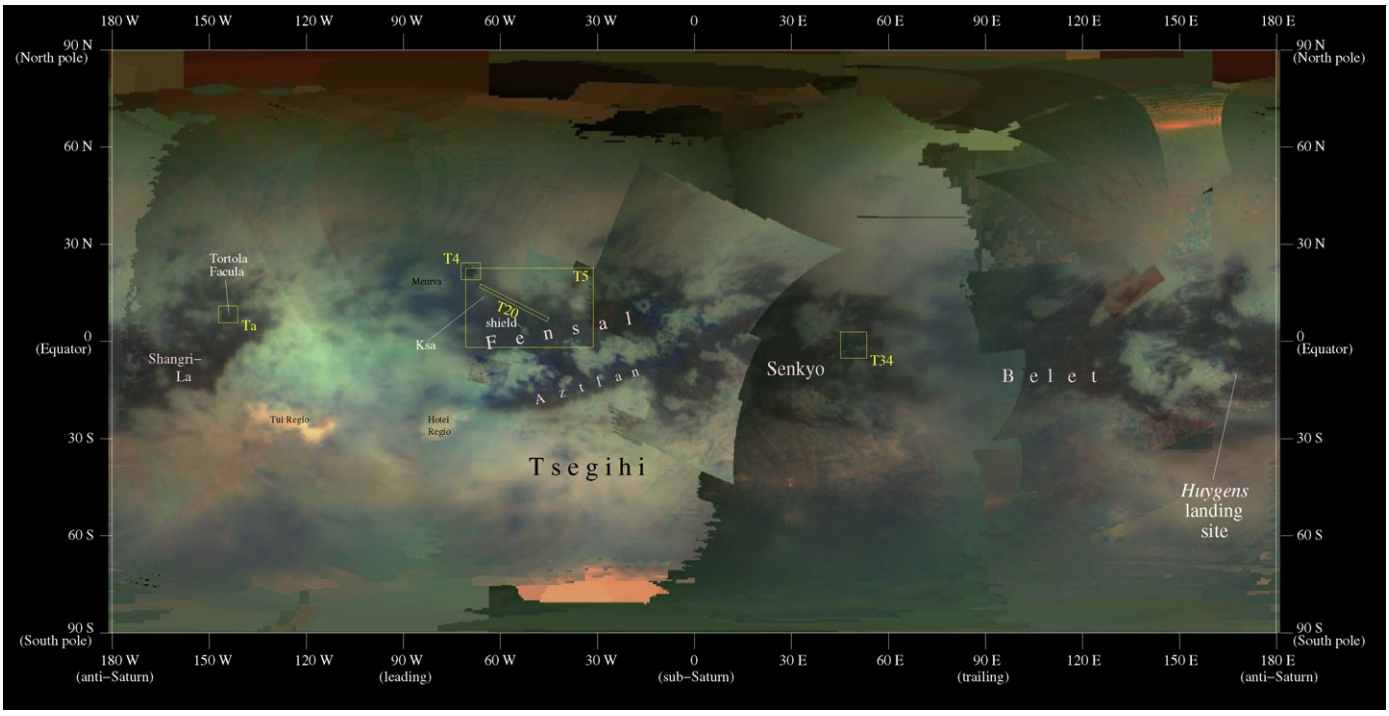

Fig. 1. Overview of the locations and observations discussed in this work. The VIMS basemap is an evolved version of that from Barnes et al. (2007a) that includes data from the T8 (2005 October 28), T9 (2005 December 26), T13 (2006 April 30), T32 (2007 June 13), T33 (2007 June 29), and T34 (2007 July 19) flybys. The red channel maps to 5 μm, the green channel to 2 μm, and the blue channel to 1.28 μm. The data are as yet uncorrected for incidence, emission, and phase angle, resulting in seams where cubes with varying geometry overlap. The observations where VIMS sees sand dunes are outlined in yellow.

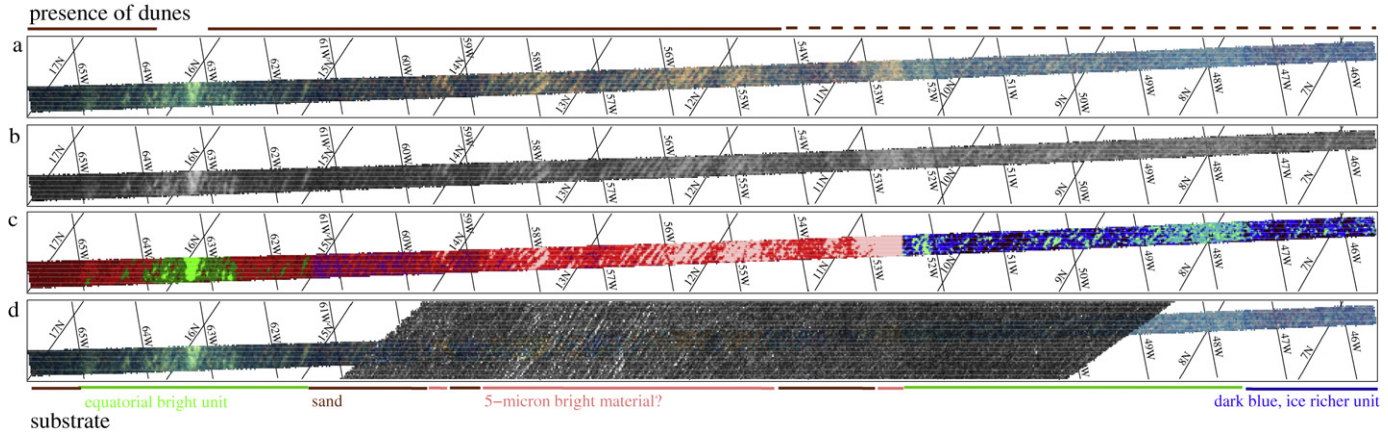

Fig. 2. The T20 12-pixel-wide swath in north-central Fensal. Here we show the geometrically projected swath rotated through Euler angles so as to result in a linear "noodle." The noodle was then squeezed in the left-right dimension by a factor of 3 to fit it reasonably into a single figure for ease of comparison across the swath. Subfigure (a) presents the data in color with red being a coaddition of 2 VIMS channels from 2.78 to 2.8 μm, green a coaddition of 4 channels from 1.98 to 2.03 μm, and blue a coaddition of 2 channels from 1.27 to 1.3 μm. The coadditions are necessary to improve the signal-to-noise ratio on these short 13 ms exposures; flux within the 5 μm window is too low to generate useful images. Subfigure (b) is a black-and-white 2 μm map. Subfigure (c) is a classification map used to derive spectra for various units, as shown in Fig. 3, and subfigure (d) shows the T20 VIMS noodle where it crosses the RADAR T17 swath as obtained from the Planetary Data System. In the VIMS/RADAR overlap region, RADAR is used for value and VIMS for hue and saturation. See Section 3 for a more detailed discussion of this figure.

measuring the spatial characteristics of the dunes in this region we utilize unaltered cylindrical maps, as described in Section 5.

The swath as seen in Fig. 2 is remarkably nonuniform in both albedo and spectrum. The general blue gradient from left to right along the swath, as seen in Fig. 2a, results from increasing atmospheric scattering as the terrain covered is illuminated with lower incidence angle at the end of the swath (26°, right) than at the beginning (46°, left). *Cassini* was approaching Titan during the observation, which started with a range to Titan's surface of 1280 km and ended with a range of 970 km. Time increases to the right, as the spacecraft passed over Titan's surface from west to east.

Based on the morphology of thin, isolated linear marks in some portions of the swath, the low albedo that would explain

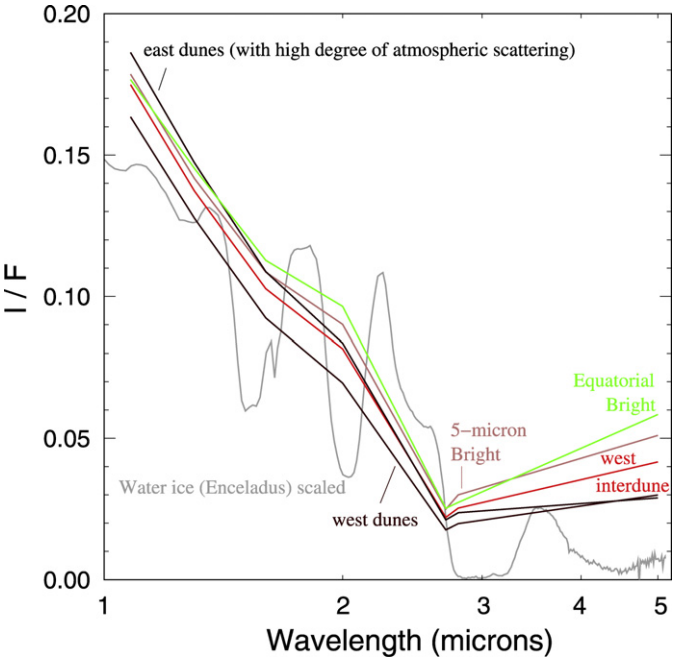

Fig. 3. Spectra of selected numerically-determined classes illustrated in Fig. 2c. Green corresponds to what we interpret to be equatorial bright substrate peeking out from between the sand dunes. Dark red represents the dunes themselves on the west end of the swath, and the upper black curve is the dunes from the east end of the swath. The difference between the two at least partially results from differences in atmospheric absorption and scattering across the swath. The red spectrum is one from transitions between dunes and interdunes, and the pink spectrum, with its spectacular 2.8 μm/2.7 μm ratio, represents 5-μm-bright interdunes. We are only able to sample the spectrum at 8 different points: 0.94, 1.08, 1.28, 1.6, 2.0, 2.7, 2.8, and 5 μm. The lines shown interpolate between those points, and as such the lines do not necessarily represent the true surface reflectivity. For an example of a full Titan spectrum with the windows identified see McCord et al. (2006) or Barnes et al. (2007a).

the dark brown spectral unit, and correlation with the SAR-dark dunes in the colocated T17 RADAR strip (Fig. 2d), we infer that the sand dunes are the dark lines in the VIMS image. The dunes are most prominent near the center of the VIMS swath, between 60° W and 52° W, but they are evident between 65° W and 64° W, between 63° W and 60° W, and in patches toward the east.

3.2. *The interdunes*

Why are the dunes more prominent in some areas on Titan than in others? To address this question, we look at the spectral characteristics of the dunes across the T20 swath. The dark areas that represent individual dunes change in spectrum only as would be expected for the corresponding atmospheric contributions along the swath (Fig. 2a, also see Fig. 3). The bright areas that sometimes show between the dunes vary significantly, though. From this we infer that the bright material between the dunes is not made of the same material that makes up the dunes. This bright material is analogous to regions within terrestrial sand seas between dunes that are sand-free, known as interdunes. The interdune material likely then represents the substrate unit that the dunes are covering.

Interdunes can be seen in many different types of dune fields, including transverse dunes, star dunes, and longitudinal dunes. A photo of an interdune from the Mesquite Dunes in Death Valley National Park is shown in Supplementary Figure 3. Interdunes on Earth can be strikingly sand-free, given their proximity to dunes of sand. The Namib dunefield, which Lorenz et al. (2006) used as an Earth analog for Titan's equatorial dunefields, is only 40–50% covered in sand, with the rest consisting of sand-free interdune regions (Lancaster, 1995). Interdunes that represent the exposure of dune substrate are common within terrestrial longitudinal dunes (e.g. in Australia; Wasson et al., 1988).

As the interdunes are not present in all parts of the T20 swath, evidently not all of Titan's dunefields possess sand-free interdunes; some have nearly continuous sand sheets or have interdunes composed of the same dark-brown spectral unit that makes up the dunes. If, for instance, the continuously dark areas within the T20 swath (like that near 61° W) had interdunes made of dark brown sandstone, VIMS would not be capable of identifying that fact.

Given the expected particle diameter within the dunes of 180–250 μm (Lorenz et al., 2006), the VIMS penetration depth given our wavelength coverage (∼10 μm), and a low albedo inhibiting multiple-scattering, if there were even a monolayer of sand particles covering what we are calling the interdune regions those areas would begin take on a dark brown appearance to VIMS. Hence the interdunes in the T20 swath must be almost entirely free of dark brown sand.

The fact that Titan presently has dunes and interdunes implies that the dunes are presently in an active state, or at least that they were active in the geologically recent past. Inactive sand seas on Earth, like the Nebraska Sand Hills, have continuous sand across their expanse. There, bedrock outcrops only where streams cut through the sand. Given sufficient time and no active aeolian processing to maintain it, the dune/interdune dichotomy would degrade from both mass wasting and from the fluvial redistribution of sand, as it did in Nebraska after the climatic shift associated with end of the most recent glaciation. That this has not occurred on Titan, at least in the area studied by VIMS on T20, indicates that active aeolian dune formation is presently occurring more rapidly than sand redistribution. Barring an unrecognized abrupt climate shift recent enough to have altered the dunes' status but not so long ago as to have allowed the new climatic regime to redistribute the sand, Titan's dunes are probably active in the present day.

Because within the interdunes we see the dune substrate, and not locally-derived sediments, these dunes likely migrated into the area from elsewhere. On Earth, low sand supply and a negative sand budget are thought to lead to sand-free interdunes. Higher sand supply and/or local sand production lead to sand-covered interdunes. This explanation is consistent with the Namib dunes. In the southern and central Namib, greater sand supply leads to sandy interdunes, while the interdunes in the north, with lower sand supply, have interdunes composed of pre-dune gravel (Lancaster, 1995).

4. Spectroscopy

4.1. Dune composition

We show a numerically-calculated spectral unit map of the T20 swath in Fig. 2c. The units are calculated by assigning a set of spectral endpoints, assigning units based on which pixels' spectra are closest to which endpoints, and then repeating the process with new endpoints assigned to be the average spectrum of each unit. We iterate in this manner until an equilibrium is reached where the map changes little or not at all between iterations. We split the swath into three separate zones for the calculation in order to limit atmospheric influence on the unit groupings.

The spectrum of the dunes (dark lines in Fig. 3) in general tracks quite well that of other parts of Titan, but with a lower albedo. In particular the dunes' reflectivity is low at 5 μm, and shows a positive 2.8/2.7 μm ratio. The dunes are decidedly darker than the rest of Titan in the short wavelength windows at 1.08 and 1.28 μm. We have omitted the 0.94 μm point from the spectrum because the dunes are not identifiable to VIMS at that wavelength due to atmospheric scattering. The fact that the dunes are relatively dark at 1.08 and 1.28 μm combined with the high 2.8/2.7 μm ratio implies that the dunes possess a relatively lower water-ice composition than the rest of Titan. We cannot, at this point without a robust atmospheric correction, rule out a small water-ice fraction.

If the dunes are not composed of water ice, at least not predominantly, then of what are they composed? The 13-ms exposures in the T20 pointing design were chosen so as to maximize the areal coverage for imaging during the flyby; hence for Fig. 3 we coadded the best VIMS channels within each spectral window. Specific identification of absorptions, like that of benzene detected within Titan's dark spectral units by Clark et al. (in preparation), require high signal-to-noise ratios, particularly within the 5-μm window, that are not possible given the T20 dataset. We discuss the observational design of a sequence that would be capable of such a detection in Section 6.1.

The dunes' low albedo in all wavelengths and overall spectral shape is consistent with a variety of carbon-bearing species, as first noted for the spectra of the dunefields as a whole by Soderblom et al. (2007). Given that the penetration depth of near-infrared photons should be of order several or at most several tens of wavelengths, this inferred organic composition is only known to be representative of the outer layer of Titan's sand particles. It is conceivable that the individual sand particles are not radially homogeneous, and that the VIMS reflectivity only represents an outer rind of organic material with a core of water-ice or other material.

Barring such a nonuniform composition, the organic signature of the sand particles is not consistent with their creation from the erosion of water-icy highlands material as suggested by Lorenz et al. (2006) and Jaumann et al. (2008). While the ultimate source of organic material on Titan's surface is photo- and radio-chemistry of atmospheric methane (e.g. Waite et al., 2007), the mechanism for generating 0.18–0.25 mm particles is not clear. Most sand on Earth is composed of SiO_2 because it is abundant in Earth's crust, chemically stable, and easily eroded into small particles via fluvial processes. However an important additional factor is that, once produced, small SiO_2 sand particles are quite strong and resistant to further erosion. The production mechanism of Titan's organic sand grains must similarly readily produce particles in the right size range, but not continue to either break those particles down or build them up past a saltatable size.

There are two ways to produce particles of a given size: by eroding down particles of larger size, or by growing smaller ones. We consider each of these possibilities below.

If the organic particles that make up Titan's sand dunes are formed by breaking down larger grains, then some source of those larger grains must have existed at one time, and may still be present. Such a source could be a geological unit of lithified solid organic material. Creation of this source would seem to require: (1) concentration of solid organic material, (2) burial and lithification, (3) subsequent exhumation and erosion. If methane rainfall were able to partition and concentrate solid organic material either by dissolution or suspension, then any given concentration of such matter could be buried and lithified by impact ejecta, tectonic activity, or other surface depositional processes. Overburden pressure and either geothermal or impact-derived heating could then drive lithification. For instance, the ejecta blanket around the titanian crater Sinlap is hundreds of kilometers wide and estimated to be tens to hundreds of meters thick (Le Mouèlic et al., 2007). Fluvial erosion through the ejecta blanket and down to the lithified-organic layer could then start the breakdown process. If this top-down hypothesis is correct, then we might expect to find outcrops of the lithified-organic layer still extant somewhere on Titan's surface.

As first suggested by one of us (R.H.B.), the alternative, bottom-up sand construction mechanism could involve the sintering together of organic haze particles on Titan's surface after they fall out of the atmosphere. Tomasko et al. (2005) estimate that haze particle radii near Titan's surface could approach 0.9 μm—still a million times smaller than predicted for the organic sand particles by mass. The time required for particles to sinter into grains of a given size r goes as r^4 (Herring, 1950). Hence growth could be naturally stalled at a given size, preventing sand dunes from sintering into one solid organic mass. Using chemical parameters for benzene, Brown et al. (2006) showed that under Titan conditions haze particles on the surface should sinter into sand-sized particles in between 10^4 and 10^8 years, depending on assumptions for the time necessary for 1-μm grains to grow to 2-μm grains. These values make atmospheric haze a possible source for the grains that make up the sand dunes. Collisions between grains could erode them, preventing grains from growing larger than sand-sized.

Under either scenario, the particles must have a high resistance to further erosion; the particles would need to be highly solid, and not gooey like organics near their melting point. Although the benzene seen by Clark et al. (in preparation) meets these criteria, so do many other compounds. The mechanical behavior of such compounds under Titan conditions is only just beginning to be explored, but initial results show a surprising

variety of characteristics (Lorenz et al., 2008). As such, the precise composition of the sand in Titan's dunefields remains an open question.

4.2. Interdune composition

Classification of the spectra of the interdunes into the global spectral unit that they best match is straightforward, given that the signal-to-noise ratio is better for these more highly reflective units than it is for the dark dunes. Our identifications are depicted at the bottom of Fig. 2. In some areas we are unable to satisfactorily identify the composition of the interdunes, perhaps because either no interdunes exist in those areas or because the interdune composition is similar to that of the sand particles themselves (and may indeed *be* sand). Those areas are designated with "sand" as the substrate unit, and are depicted in brown. Some of the "sand" areas look like they might be extensions of nearby substrate units but with a higher sand cover; the distinction between identifying those best-guess substrates and calling the areas "sand" is arbitrary.

Near the west end of the swath, at 15.9° N 63.2° W, is an outcrop of the equatorial bright spectral unit [as described in Barnes et al. (2007a); this unit corresponds to the bright neutral unit from Soderblom et al. (2007) near the equator] 5–10 km across. This unit's reflectance matches that of most of the bright material within 25° of Titan's equator (except for Xanadu), and shows up as greenish in the $R = 2.8$ μm, $G = 2.0$ μm, $B = 1.28$ μm color scheme shown in Fig. 2 [as well as with the same color scheme but $R = 5$ μm as in Barnes et al. (2007a)]. This particular small outcrop is free of dunes. On either side of the equatorial bright patch are areas that have dark linear sand dunes crossing on top of what evidently is a continuation of the equatorial bright spectral unit. The dunes here generally cover a greater areal fraction the further one progresses from the equatorial bright patch. About 50 km away from the equatorial bright patch in both directions the dunes start to dominate, covering enough of the underlying material so as to make unambiguous identification of its spectral unit challenging. The classes that we interpret to correspond to the equatorial bright unit in the west end of the swath here are colored green and dark green, and the spectrum of the green class is shown in Fig. 3.

Progressing eastward down the T20 swath, as *Cassini* did, we next encounter interdunes near 59.5° west longitude. In a small patch here and then in larger patches toward the east until 52.5° W, the dunes and interdunes contrast strongly and the interdunes have very different reflective properties than the interdunes did further west. These interdunes, algorithmically mapped as the pink spectral class in Fig. 2c, are bright at 5 μm and have a very large 2.8 μm/2.7 μm ratio. Both of these characteristics, but particularly the latter, identify them as belonging to the 5-μm-bright spectral unit that was first described by Barnes et al. (2005) and is also explored in Barnes et al. (2006), McCord et al. (2006), and McCord et al. (2008). To see such small outcrops of the 5-μm-bright unit so far from Tui Regio and Hotei Regio surprised at least one of us (J.W.B.). This portion of the swath evidently represents older 5-μm-bright terrain that dunefields have either encroached into and have now fully covered, or an area that used to be entirely covered by sand that is now being removed, exhuming 5-μm-bright terrain. This interpretation is consistent with regional spectral mapping and solves a dilemma that has stood since the T5 Titan encounter on 2005 April 16 as we describe below in Section 4.3. Furthermore, if all 5-μm-bright material is similar, then the RADAR swath that covers this area, that from T17 shown in Fig. 2d, may give us a preview of what RADAR might see when and if that instrument obtains coverage of Tui Regio and/or Hotei Regio, only without the dunes. The 5-μm-bright interdunes are quite bright in 2.2-cm synthetic aperture radar, implying that they are either texturally rough at several-centimeter length scales or that they are highly fractured and therefore highly volume-scattering.

The area with 5-μm-bright substrate beneath the dunes ends abruptly at 52.5° W. The VIMS imaging becomes less coherent as we move eastward from here as a result of the downtrack spacecraft velocity increasing past the point where the instrument can complete a full 12 pixel line before traveling 1 pixel downtrack. Immediately eastward of 52.5° W is an area that may again be underlain by equatorial bright material where it is not entirely covered by sand. At the far eastern end of the swath, eastward of 47° W, the dunes may overlie an instance of the water-ice-enhanced dark blue unit that *Huygens* landed on first identified by Rodriguez et al. (2006) and also explored by McCord et al. (2006), Soderblom et al. (2007), and Barnes et al. (2007a).

The nature of the substrate as seen between dunes is uncertain. Classical interdunes are flat plains between dunes. The interdunes that we see could be similar. They could also be topographic highs that have dunes climbing up through them. The VIMS data are insufficient to answer this question, and it will therefore need to be addressed by future observations, probably post-*Cassini*.

4.3. Regional context

We attempt to make sense of the substrate spectral units that VIMS encountered in the T20 swath by placing the swath into regional context. The observation with the best combination of resolution, phase angle, and uniformity of coverage surrounding the T20 swath was that on T5 (2005 April 16). We show the T5 data and the T5 data along with the VIMS T20 swath and annotations in Fig. 4. The T5 data have been forcibly registered to the Ta RADAR swath in absolute geometry—however, their inherent resolution, T20 ephemeris uncertainties, and recent discoveries regarding the location of Titan's rotational pole (Persi Del Marmo et al., 2007; Stiles et al., 2007) mean that both the positions and the relative position of the T5 data and the T20 strip are uncertain by up to ∼1°.

The T20 swath begins north of Ksa crater in northern Fensal. The portion of the swath west of 60° W has poor VIMS coverage, as do most areas surrounding 90° W, particularly the vicinity of the crater Menrva west of Ksa. However, it seems that the T20 strip begins within an instance of the dark brown spectral unit just east of the as-yet-unnamed facula north of Ksa and east of the dunes from T4 shown in Barnes et al. (2007a).

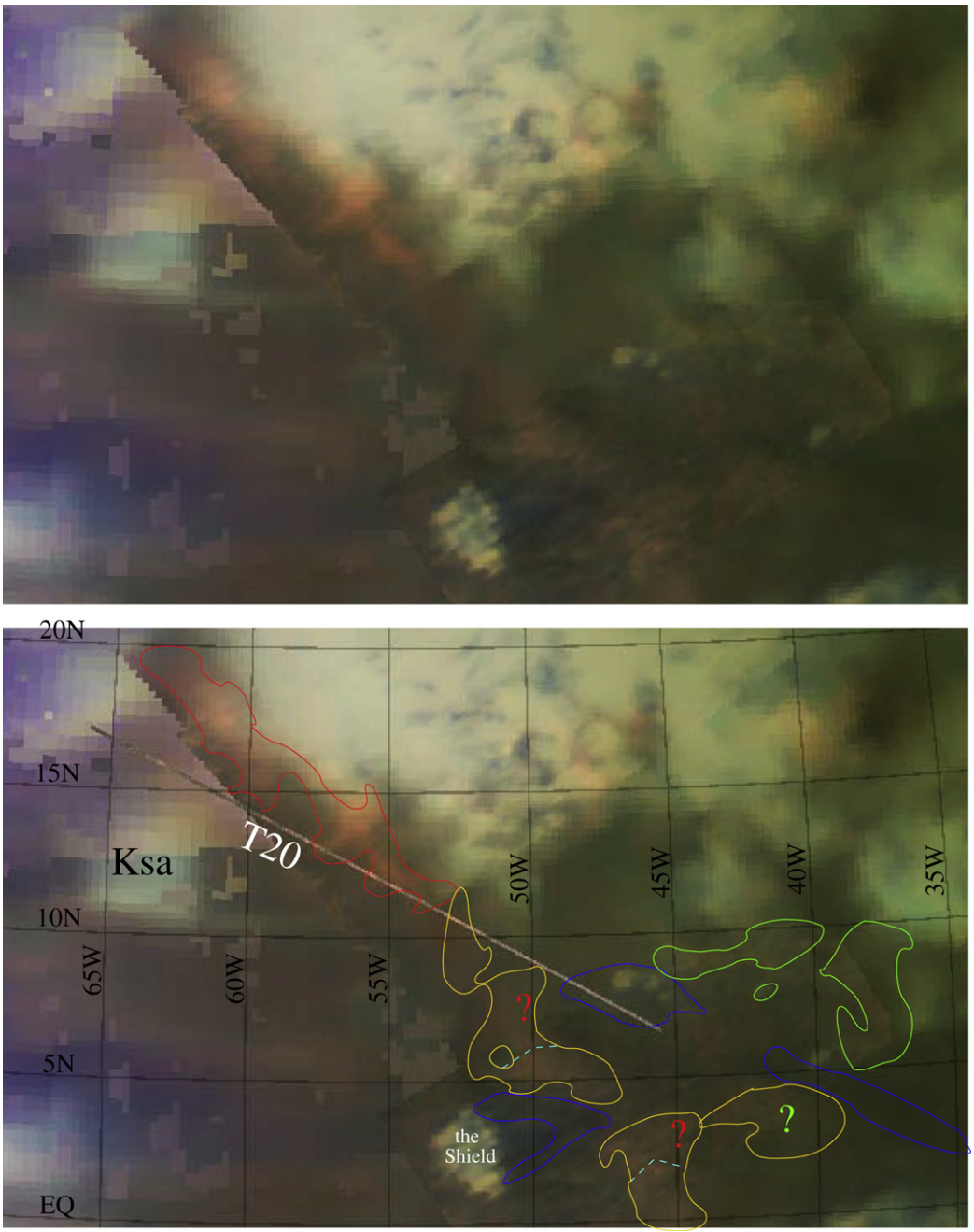

Fig. 4. Orthographic projection of a geometrically-corrected mosaic of VIMS' T5 flyby data to provide context for the long, narrow T20 swath. Red is assigned to be 2.8 μm, green as 2.0 μm, and blue as 1.28 μm. The T20 swath is included along with various other annotations in the bottom subfigure. The colored outlines delineate the extent of spectral provinces that can be seen through the dunes. The outlined provinces with question marks inside them are less certain; see text.

The equatorial bright spot within the strip could represent the edge of Ksa or perhaps a mountainous ejecta block from Ksa similar to those seen surrounding Sinlap (Radebaugh et al., 2007).

Proceeding east into moderate-resolution (6 km/pixel) T5 coverage, we see that the portion of the swath with 5-μm-bright interdunes shows up as a ghostly dark red in the regional image. This solves a dilemma regarding this area that dates from the T5 flyby: what are these darker 5-μm-bright areas with fuzzy boundaries in northern Fensal? The type units for 5-μm-bright terrain, Tui Regio and Hotei Regio, are much brighter and have sharp boundaries. Initial thinking that these might represent low-optical-depth fog was dispelled when subsequent observations also showed the ghostly dark red, albeit at lower resolution. The high-resolution VIMS T20 observations unambiguously solve the dilemma: the dark red areas represent dark brown dunes covering a 5-μm-bright substrate. The macroscopic mixing of the two results in a dark red color when viewed with spatial resolution too coarse to separate dunes from interdunes. Thus far, then, when viewed at fine spatial resolution, the 5-μm-bright unit and the dark dunes each appear to represent spectral endmembers.

This realization opens the door for the interpretation of brightness and color variations within the dark brown dune-containing spectral unit across Titan. Such an interpretation must start with the assumption that the spectrum of the dune-forming sand is uniform across the surface. While this must be mostly true based on the dune-dark brown correlation discovered by Soderblom et al. (2007), it is not necessarily true in detail. Lancaster (1995) notes that sand coloration in visible wavelengths changes significantly even within the relatively small (~100 km wide) Namib dunefield. While Mars' uniform dust gets globally distributed by storms every few martian years, Titan's saltating sand does not. The global uniformity of Titan's sand remains to be tested. Previous spectral imaging studies of terrestrial dunefields have shown that it is possible to map sand composition from remote sensing (White et al., 2001).

With the uniform-sand-spectrum assumption in place, variations within the dark brown spectral unit would then result from differences in (1) substrate composition and (2) fractional sand coverage. Given a proper atmospheric correction, high signal-to-noise, and the identification of spectral endmembers, both of these factors could be mapped within the dark brown units globally. One technique capable of such mapping would be that of spectral mixture analysis, previously applied to Titan by McCord et al. (2008). We show a manual, visual attempt to do so in Fig. 4.

While the area immediately east (presumably downwind; Lorenz et al., 2006; Radebaugh et al., 2008) of the unnamed facula that we call "The Shield" centered at 52.5° W 2.5° N is an instance of dark blue terrain (a general trend noted by Soderblom et al., 2007; McCord et al., 2008; and Barnes et al., 2007b), the dark blue wake does not have a sharply-defined edge. Its gradient toward dark brown results from dune encroachment as the dunefields try to re-form in the lee of a topographic obstacle as noted by Lorenz et al. (2006) and the sand coverage fraction increases. There is another dark area of dunes that perhaps might have a dark blue icier substrate further east of the shield. This long, thin, snaky area continues east from the edge of Fig. 4. A last area of dunes that might possibly be underlain by dark blue material is located near the end of the T20 swath. The identification here is more ambiguous—there could be equatorial bright or perhaps a different spectral unit entirely that serves as the dune substrate at the end of the T20 swath. Pitman et al. (in preparation) estimate a 30% water-ice content for an instance of the dark brown spectral unit that they measured from lower-resolution T20 observations—this value may not directly represent the composition of the dunes' sand, but may instead represent, say, 20% dune coverage over the dark blue spectral unit.

The green outlines in Fig. 4 represent areas that may be underlain by equatorial bright terrain, and the red outlines show the area with 5-μm-bright terrain underneath it as revealed by T20. The yellow-outlined zones are more ambiguous. The northern end of the yellow outline was revealed to be 5-μm-bright beneath the dunes by T20. However, the southern portions are a slightly different color, and thus may not be in quite the same situation. At least two dark, possibly bluish lineaments cross the yellow outlines as shown within the yellow outlines. These may represent channels (Barnes et al., 2007b) within the dune covered areas; higher resolution and higher integration times would help to test the channel hypothesis.

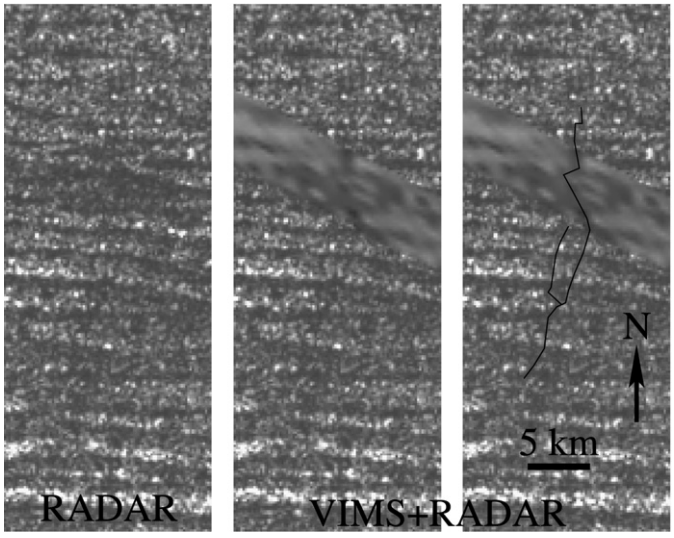

Fig. 5. Closeup view of a possible channel located within the VIMS T20/RADAR T17 dunes. RADAR view at left, VIMS 2-μm map over top of RADAR in the middle, and annotated at right. The geographic location of this view is indicated in Fig. 6.

One possible channel feature, not directly visible in the T5 context map, apparently does cross the T20 swath. When comparing the T20 VIMS observation and the T17 RADAR swath, a dark, meandering lineament is evident, as shown in Fig. 5. This feature, perhaps a pixel or two wide (~350 m), is at the resolution limit of both instruments and is particularly subtle. Its detection with both instruments makes it decidedly more believable. The putative channel runs with a north–south orientation. It crosses several sets of dunes and interdunes, intersecting them nearly perpendicularly in most cases. That VIMS can see the channels means that they are not buried structures like those seen by radar in the Sahara; or if they are buried they have a significant surface expression. That the channels and dunes coexist in this location implies that they either are or were concurrently active or that the channels are relics of the substrate material that has been overprinted with dunes.

5. Morphometry

Where the dunes are sufficiently contrasting and resolved, we are able to measure their spacing and orientation. Dune spacing can be an indicator of smaller-scale dune shapes and formation environment, and their orientation ought to be parallel to the time-averaged vector-sum wind direction. Radebaugh et al. (2008) performed similar measurements using RADAR data. While RADAR's greater fine-resolution areal coverage makes for more extensive capabilities for these studies, the VIMS data are complementary in that they cover some areas not covered by RADAR.

We show a 2-μm non-stretched version of the VIMS T20 swath in Fig. 6. Annotations indicating the presence of dark

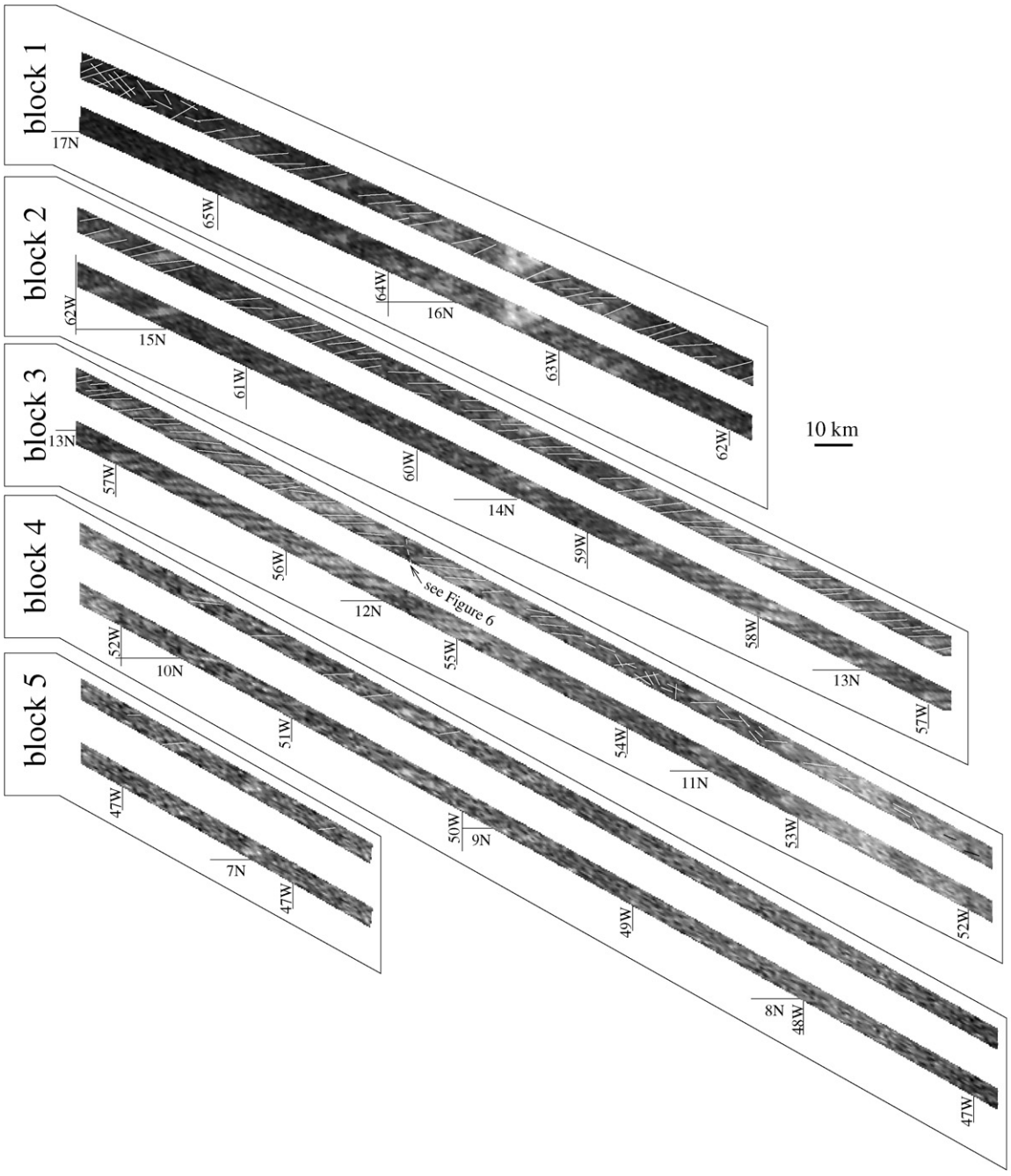

Fig. 6. The same T20 swath shown in Fig. 2, but this time in simple cylindrical projection and with just the 2-μm coadded channel shown. Block 1 is the furthest west; its eastern end overlaps with the west end of block 2, and so on down to block 5. Apparent dune locations are indicated directly above clean images. For ease in dune identification each block has been stretched independently.

lineaments are shown above unannotated images. Each block is individually stretched to enhance small-scale features like the dunes; hence intercomparison of albedos between blocks is not valid. The east–west trending lineaments are dunes. The indicated lineaments that are parallel to the swath itself are suspect—we think that they are probably artifacts resulting from the nature of the observation style and the low signal-to-noise ratio in the dark portions of the swath.

Counting 19 dunes between 14° N and 15° N, 23 between 15° N and 16° N, and 22 between 16° N and 17° N yields averages of 2.37, 1.96, and 2.05 km for dune spacings respectively, or 2.11 km as a total average. The orientations of the dune crests in block 2 show an average angle that is nearly parallel to the equator, only 2° north of east, but with wide variations between ±11°. Those in block 3 angle 5° south of east. The wide variance in orientation over this relatively small distance could be indicitive of local topography affecting average wind direction and dune orientation.

Though no other VIMS observations have such fine spatial resolution as T20, dunes or indications of dunes are seen on other flybys. The T4 dunes shown in Fig. 7, first reported by Barnes et al. (2007a), are remarkably uniform in orientation and

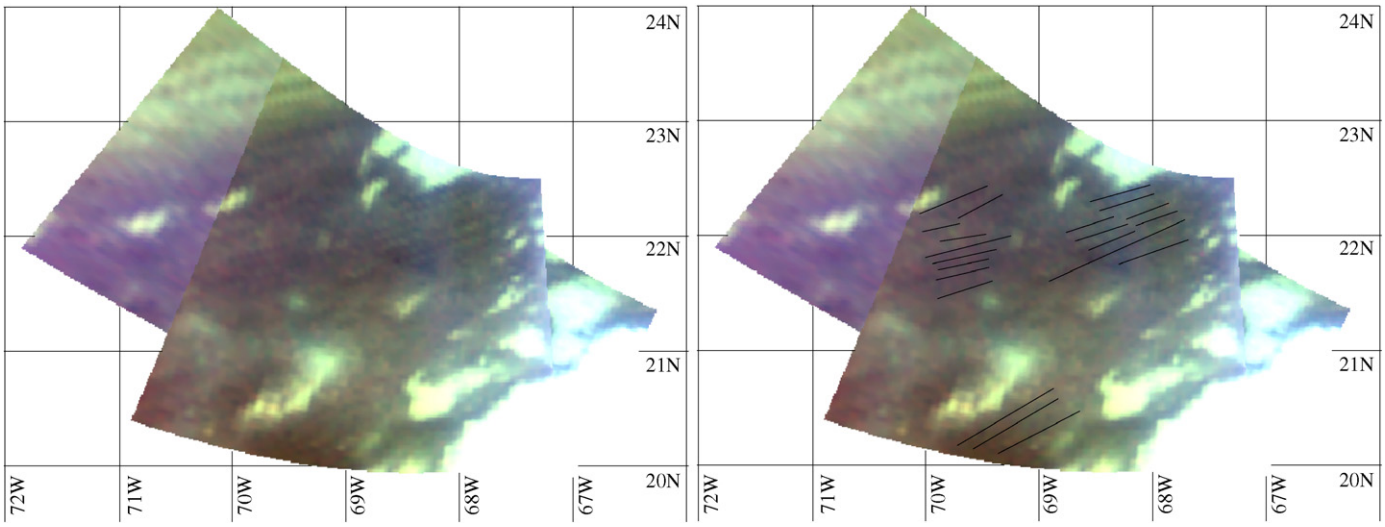

Fig. 7. High-resolution color map with $R = 2.8$ μm, $G = 2$ μm, $B = 1.28$ μm of dunes in northwestern Fensal from T4. Dune locations and orientations are indicated at bottom.

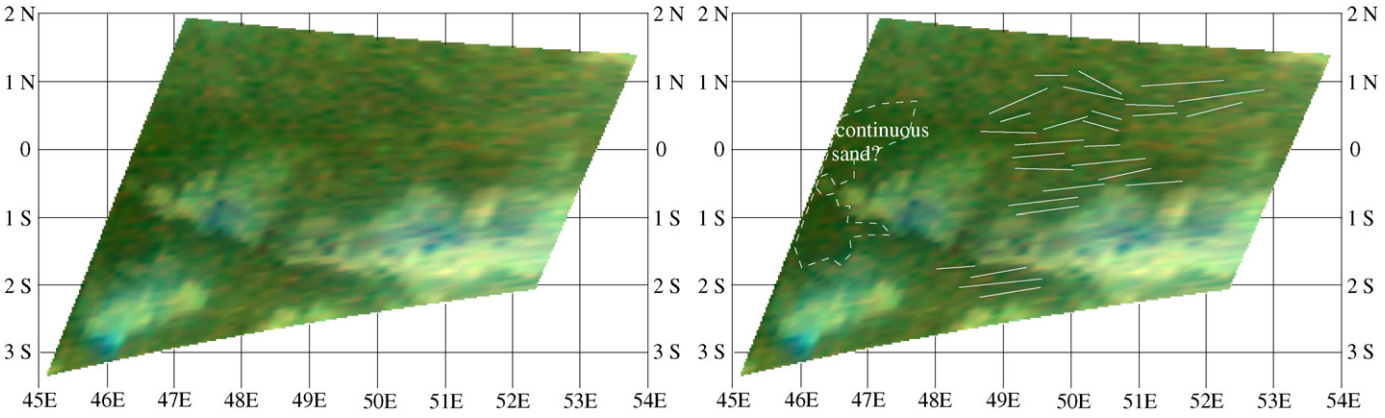

Fig. 8. Portion of the T34 "noodle mode" swath that contains lineaments that may be related to underlying dunes. See text.

spacing when compared to those from T20. They also show low contrast, implying that they either do not have interdunes or that their interdunes have similar reflective properties to the sand itself. Individual dunes are barely resolved, so in some cases the apparent dune spacing is affected by which pixel the dune itself falls onto. We calculate a median dune spacing of 2.1 km for the dunes surrounding 22° N 68° W, and a nearly uniform orientation of 17° north of east.

East–west trending lineaments are also seen on the recent T34 Titan flyby. The resolution of the observation shown in Fig. 8 is 2.7 km/pixel, which is too coarse to resolve dunes based on their separations as measured from T20 and T4 above. The lineaments indicated could be dunes with longer spacing than the others, but we think that it is much more likely that they are an aliasing effect of seeing, for instance, two dunes and an interdune in one pixel and one dune and two interdunes in the next. The lineament orientations may therefore be indicitive of the underlying dune orientations. The average orientation for T34 is 3° north of east, but with a huge variation between ±25°. The high variation likely results from the aliased nature of the lineations themselves, and is therefore unlikely to be meaningful. The average we calculate may correspond to the average orientation for the dunes in the area; however higher resolution VIMS or RADAR observations would be needed to verify the validity of orientations from coarse-resolution data.

The equatorial bright Tortola Facula, observed by VIMS at fine resolution on Ta and studied by Sotin et al. (2005), is surrounded by an instance of the dark brown spectral unit that ought to be filled with sand. However while numerous lineaments are seen in the dark brown material, few have the characteristic spacing expected for sand dunes. The spatial resolution is insufficient to resolve the dune separations. The solid lines that we show in Fig. 9 might represent dunes; the dashed lines probably do not. The area seems to have sand-colored interdunes, and is illuminated from more nearly overhead than the T4 observation; hence it should show low dune contrast. It may also be that the dunes are less regular in this area, and hence less easily identified.

A summary of our measurements from VIMS dune observations is shown in Table 2. Our spacing determination of 2.1 km is consistent with the "dunefields" designation from Radebaugh et al. (2008), and not with what Radebaugh et al. (2008) call "sand seas." The closer, ∼1 km spacing noted by those authors for "sand seas" would apply better to areas that we show having

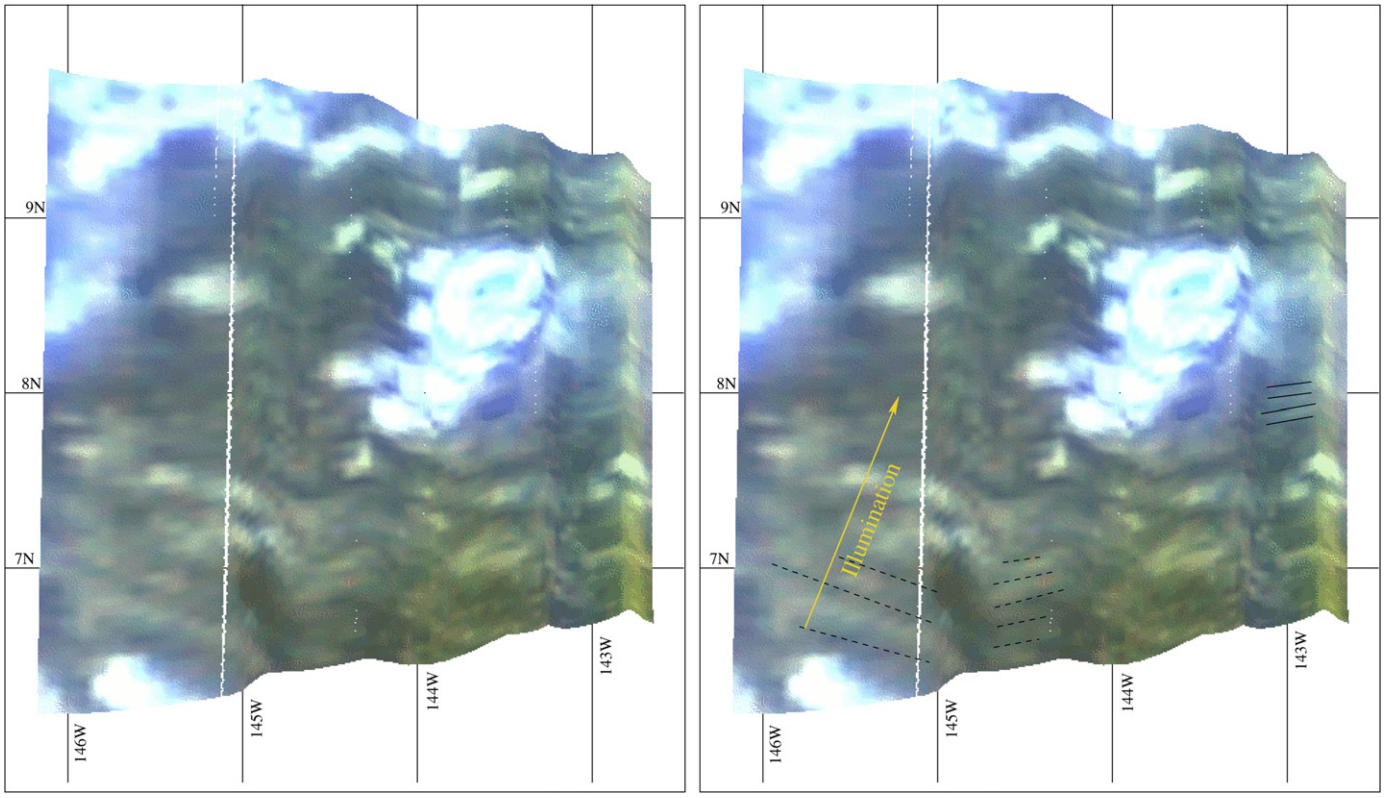

Fig. 9. This is the fine-resolution VIMS image of Tortola Facula from Ta made famous by Sotin et al. (2005), stretched instead to bring out detail in the surrounding dark brown unit. No clear duneforms are seen; the image has insufficient spatial resolution to detect them.

Table 2
VIMS dune measurements

Flyby	Location	Spacing	Orientation	Height
T20	Fensal, east of Ksa crater	2.1 km	Block 2: 2° N of E	–
T20			Block 3: 5° S of E	–
T4	NW Fensal, west of Bali Facula	2.1 km	17° N of E	30–70 m
T34	Eastern Senkyo	–	3° N of E	–
Ta	Surrounding Tortola Facula	–	10° N of E (?)	–

Note. Spacing measurement is the median spacing from several measured dunes. Heights are derived from photoclinometry, where valid; the measured values probably contain unquantified systematic errors that render the results as only approximations.

a "sand" substrate. The RADAR measurements of dune orientations are more extensive that those we present here both in quantity and area covered. Our determination that the dunes are oriented mostly east–west with local variability away from that value is consistent with Radebaugh et al. (2008). Crest-to-crest dune separations are strikingly similar to those seen in the Namib desert Lancaster (1995), as first noted by Lorenz et al. (2006).

6. Photoclinometry

To constrain the crest-to-trough height of Titan's sand dunes, we employ photoclinometry (also known as "shape from shading"). The technique takes advantage of the fact that terrain facets with orientations more nearly perpendicular to the illumination direction appear brighter than those facets facing away from the Sun. Each pixel can thereby be assigned a maximum slope. By integrating these inferred slopes along a line parallel to the illumination direction, we assemble a topographic profile.

In order for brightness variations in an image to represent slope, the albedo across the scene must be uniform. Hence the VIMS observations of dunes that are separated by interdunes that have albedos characteristic of the substrate material, as in the T20 strip, are not appropriate for the application of the photoclinometric technique. Our observations from Ta, T4, and T34 contain areas where the region between dunes is either covered in sand or of a material with the same spectral properties. The signal-to-noise ratio and resolution of the T34 observation, however, are insufficient for photoclinometry in the region where the albedos are appropriate. The Ta observation, despite good illumination from the south at 30° zenith angle, does not show repetitive dune-like structure even though it is dark brown and shows evidence of east–west trending "ridges" (Sotin et al., 2005). Hence we focus our photoclinometric analysis on the 80-ms-integration 64 × 64 cube with dunes from T4.

We use a one-dimensional photoclinometry algorithm that was written for evaluating martian landing sites (Beyer et al., 2003), but that has since been used to measure topographic profiles of both aeolian (Bourke et al., 2006) and subaqueous (Burr et al., 2004) martian dunes, as well as profiles of Europan ridges (Hurford et al., 2005). The algorithm is detailed in Beyer et al. (2003), but we summarize the relevant aspects and Titan modifications here. When previously applied to martian imaging, Beyer et al. (2003) applied the photoclinometry algorithm to calibrated geometrically raw images to reduce systematic errors. Since VIMS is a spot-scanner and our resolution and viewing angles vary significantly over the course of the T4 cube, raw-geometry cubes are not effective for photoclinometry. Hence after calibration (see Section 2), we project the relevant cubes into a simple cylindrical coordinate system as outlined in Barnes et al. (2007a), using nearest-neighbor interpolation to best preserve photometric properties.

We use just the 2 μm band (VIMS plane number 165 in a zero-offset c-style numbering system) to optimize signal-to-noise ratio while minimizing atmospheric effects. Though atmospheric scattering from haze particles is reduced in the 2 μm band, it is not eliminated entirely. We subtract from the image an empirically determined constant to compensate. The assumed atmospheric value is one source of systematic error associated with the resulting topographic profile. For the surface photometric function, we assume a Henyey–Greenstein phase function with $g = -0.4$ as determined by Buratti et al. (2006) for Titan's low-albedo areas. As this function was measured for broad dark areas that include both dark brown (sandy) and dark blue (icy) terrains, and because the function was measured for much lower spatial resolution and thus characterizes larger-scale slopes than those of interest in the T4 cube, it is also a likely source of systematic error. We run a forward-solution for what values of I/F would be expected for pixels as a function of surface slope angle with the observation's given photometric angles, and for each pixel in the profile we look up that pixel's measured I/F in the table and interpolate to find its slope.

The profile and its location are shown in Fig. 10. To minimize systematic errors driven by non-uniform albedo, we chose an area that appears spectroscopically to have either sand-covered interdunes or ones with similar spectral properties to the dunes themselves. To compensate for residual albedo variations on scales larger than that of the dunes themselves (like that around kilometer 44–50), we high-pass filtered the profile using a wavelet transform. The wavelet transform introduces artifacts at the start and end of the sequence that it transforms, so we show only the interior portion of the profile not affected by the artifacts.

Not every bump in the profile represents a sand dune, necessarily. The most robust dune detections, such as those between kilometers 28–40 and 50–60 in the profile, show crest-to-trough dune heights of between 30 and 70 m.

This VIMS photoclinometric dune height measurement is smaller than the RADAR determination of 100–150 m in Belet from photoclinometry. This is likely due at least in part to the different nature of the dunes in the VIMS location relative to those in Belet: the dunes measured by RADAR were the most spectacular, highest-contrast dunes seen; the VIMS dunes are decidedly more modest when viewed both with VIMS and with RADAR from T3 [see Fig. 10 from Barnes et al. (2007a)]. As mentioned in Section 3, areas such as that covered by the VIMS T4 cube that have no interdunes may be covered in more complicated complex or composite dune structures. The VIMS T4 area may also represent one with a different dune-formation regime, either with differing wind conditions or sand supply, which may also account for the discrepancy. Given the diversity that occurs even within individual sand seas on Earth (Lancaster, 1995), it is perhaps unsurprising that Titan's dunefields are showing a high degree of diversity as well.

6.1. Future observations

While the T4 observations allowed an estimate of dune heights, those observations are limited by coarse spatial resolution. A more robust estimate would require at least 2 and preferably more pixels across the dune itself, or more like 5–8 pixels between each dune crest.

A dune profile would allow us to identify whether the dunes are presently active and to ascertain the wind regime in the present season. Active longitudinal dunes, such as those in the Namib (Lancaster, 1995), develop slip faces on the downwind side of their crests. The slip face changes direction (and often length) when the winds change seasonally. Though the average wind direction is generally west-to-east (Lorenz et al., 2006; Radebaugh et al., 2008; and Section 5) the instantaneous wind direction probably alternates between extremes as is characteristic of other longitudinal dunefields. Perhaps the surface winds near the equator blow from the northwest in southern summer, and then from the southwest in northern summer, for instance. A topographic profile with sufficient resolution would be capable of identifying the present state of the dunes and, if slipfaces are found, the present wind regime.

Given the necessary resources and the desire to do so, VIMS is capable of profiling the dunes' slopes before the end of *Cassini*'s mission. Obtaining 5–8 pixels across a dune would require high resolution of better than 400 m/pixel, and thus an observation near closest approach like the one studied by Jaumann et al. (2008). VIMS would need to be oriented such that hi-res mode would improve the resolution perpendicular to the dune orientation. The observation would require high signal-to-noise, and thus at least an 80 ms exposure time, preferably 160 ms, for reliable photometry of the dark dunes. Parts of the Belet sand sea might be appropriate to target.

Finally, such an experiment would require an appropriate target with optimized geometry. We would need to target an area with known dunes and, if possible, one known to have sand-covered interdunes. The dunes would preferably fill the VIMS field of view, thus maximizing the potential profile length. They should occur at the proper local solar time such that the down-Sun direction is perpendicular to the dune orientation. The spacecraft should be oriented such that VIMS' sample direction is parallel to the illumination direction. Finally, the solar

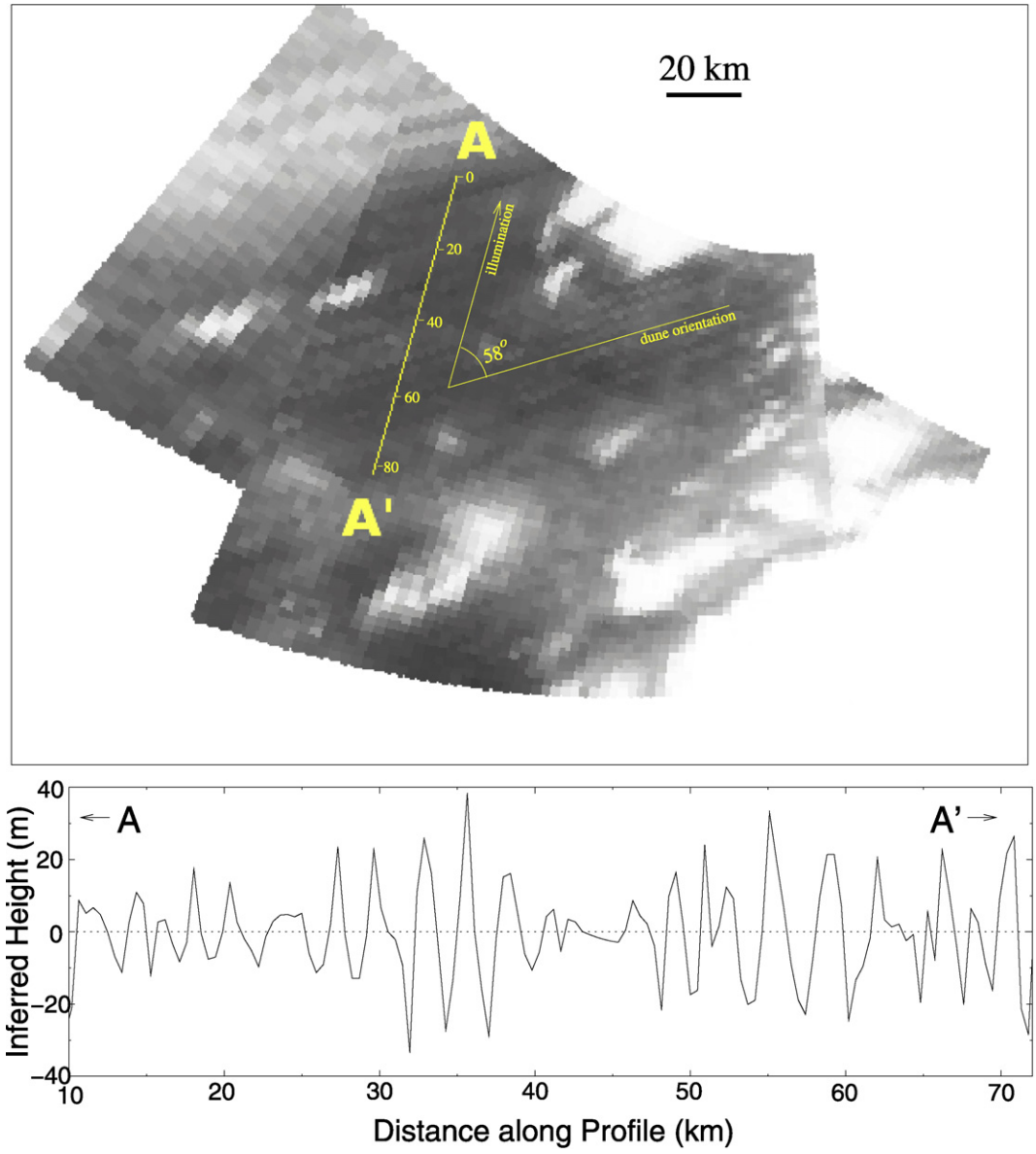

Fig. 10. A simple-cylindrically projected, highly stretched 2-μm image of dunes west of Bali Facula obtained by VIMS during the T4 *Cassini*—Titan encounter is shown at top. The insolation incidence angle is 45°, the emission angle is 4°, and the insolation direction is toward 16° east of north. The image is centered at 20° N 68° W. A photometrically-determined topographic profile between points A and A', shown is shown below. In order to eliminate topographic and albedo variation on scales much larger than the dunes, the profile has been high-pass filtered using a wavelet transform (Press et al., 1992) to emphasize structures smaller than 5 km in spatial wavelength.

zenith angle should be maximized. Given that Titan is heading into equinox in 2009, the zenith angle constraint means that the target dunes must be as far as possible from the equator. They should be as far north as possible if the observations were taken before 2009, and as far south as possible if they were taken after.

The cube obtained need not be a full 64 × 64 pixels in lateral extent. While the hires, cross-dune sample-direction should be the full 64 pixels, the minimum number of lines necessary would be enough so as to provide imaging context for the obtained profiles: of order ∼10 lines minimum.

A long exposure within the dunes would also have the ancillary benefit of further constraining the dunes' composition. These observations would have pixels known to contain sand with a high filling factor, and their high signal-to-noise ratio would allow for a robust search for absorption lines within the 5-μm window.

7. Conclusions

The *Cassini* Visual and Infrared Mapping Spectrometer has developed a novel mode of data acquisition that allows observations near closest approach, when the spacecraft is moving over the surface too quickly to focus on the ground. We call it "noodle mode." The instrument repeatedly acquires lines of spectra oriented perpendicular to the relative motion of the spacecraft

and the surface beneath it. Using this technique during the 2006 October 25 closest approach with Titan (T20), the instrument acquired data with a high duty cycle and a maximum spatial resolution of 485 m/pixel.

The closest-approach observations lie in northern Fensal, within a dark brown spectral unit known from RADAR to contain longitudinal sand dunes. VIMS is able to identify the dunes. They are dark in each of Titan's spectral windows, showing high contrast in some places and low contrast in others. We infer that the areas of high contrast are in fact areas where the dunes overlie a chemically distinct substrate that shows through in the interdune areas. The interdunes are almost entirely sand-free, similar to interdunes on Earth.

These observations are the first to acquire unadulterated spectra of the sand that makes up the dunes. Those spectra indicate that the dunes' sand is not made of pure water ice. Though some small water ice component cannot be ruled out, the moderately high 2.8 μm/2.7 μm ratio and relative intensity between the 1.08, 1.28, 1.6, and 2.0 μm windows reveal the sandy spectral endmember to possess a lower relative water-ice content than Titan's average. The specific identity of the remaining component remains unknown, but given the spectral constraints and Titan's chemistry, some combination of organic compounds seems likely.

The mechanism for generating 200-μm-diameter organic particles that can saltate and form dunes is not known. An erosional process like that on Earth would require a lithified source of solid organic material that is capable of being eroded. Construction of particles from smaller haze particles, perhaps by sintering, must be able to both grow particles rapidly but halt their growth at the correct particle diameter.

Resolving the dunes results in spatial separation of dune and non-dune spectral endmembers. We have identified and mapped the substrate spectral units that underly the dunes throughout the T20 swath. Equatorial bright substrate dominates at the westward and possibly the eastward ends of the swath. The middle of the swath shows 5-μm-bright interdunes. These are the first instances of 5-μm-bright terrain known outside of Tui Regio and Hotei Regio. Their presence explains the fuzzy-bordered dark red spectral unit seen in northwestern Fensal on T5 to be a macroscopic mixture of dune and 5-μm-bright spectral endmembers. Hence the subtle, but real, spectral and albedo variability within Titan's dune-filled dark brown spectral unit likely results from variations in fractional sand cover and substrate composition. We have shown that the identity of the substrate can be determined in those cases where dunes cover a sufficiently small fraction of each pixel. Future work entails doing this more thoroughly and quantitatively.

We measured the typical dune spacing to be 2.1 km. The dunes are oriented predominantly east–west, with variations of about 10° in either direction. In areas that show sand-colored interdunes or no interdunes at all, we were able to use photoclinometry to ascertain the dunes' height. Our measured value of 30–70 m is significantly lower than that measured within Belet by Lorenz et al. (2006). We suggest that the discrepancy could be the result of the fact that the dunes that we measured appear ordinary when seen by RADAR, while the dunes that RADAR determined the heights for radarclinometrically in the sand-rich sand sea Belet are the most spectacularly high on Titan.

In short, we find that Titan's dunefields are highly variable in coverage, height, and in the terrain that they cover. We suggest future VIMS fine-resolution, closest-approach observations of dunes in order to measure their slope profile. A discontinuous profile could represent a slipface, indicating that the dunes are presently active and revealing the instantaneous wind direction. The proposed high integration times would also serve to constrain the sand's composition by providing a sufficiently high signal-to-noise ratio to search for absorptions within the 5-μm window.

Acknowledgments

This work was supported by the NASA Postdoctoral Program (administered by Oak Ridge Associated Universities for NASA) and the *Cassini* Visual and Infrared Mapping Spectrometer science team. It was partly performed at the Jet Propulsion Laboratory, California Institute of Technology, under contract to the National Aeronautics and Space Administration.

Supplementary material

The online version of this article contains additional supplementary material.

Please visit DOI: 10.1016/j.icarus.2007.12.006.

References

Barnes, J.W., Brown, R.H., Turtle, E.P., McEwen, A.S., Lorenz, R.D., Janssen, M., Schaller, E.L., Brown, M.E., Buratti, B.J., Sotin, C., Griffith, C., Clark, R., Perry, J., Fussner, S., Barbara, J., West, R., Elachi, C., Bouchez, A.H., Roe, H.G., Baines, K.H., Bellucci, G., Bibring, J.-P., Capaccioni, F., Cerroni, P., Combes, M., Coradini, A., Cruikshank, D.P., Drossart, P., Formisano, V., Jaumann, R., Langevin, Y., Matson, D.L., McCord, T.B., Nicholson, P.D., Sicardy, B., 2005. A 5-micron-bright spot on Titan: Evidence for surface diversity. Science 310, 92–95.

Barnes, J.W., Brown, R.H., Radebaugh, J., Buratti, B.J., Sotin, C., Le Mouelic, S., Rodriguez, S., Turtle, E.P., Perry, J., Clark, R., Baines, K.H., Nicholson, P.D., 2006. Cassini observations of flow-like features in western Tui Regio, Titan. Geosphys. Res. Lett. 33, doi:10.1029/2006GL026843. 16204.

Barnes, J.W., Brown, R.H., Soderblom, L., Buratti, B.J., Sotin, C., Rodriguez, S., Le Mouèlic, S., Baines, K.H., Clark, R., Nicholson, P., 2007a. Global-scale surface spectral variations on Titan seen from Cassini/VIMS. Icarus 186, 242–258.

Barnes, J.W., Radebaugh, J., Brown, R.H., Wall, S., Soderblom, L., Burr, D., Sotin, C., Le Mouèlic, S., Rodriguez, S., Buratti, B.J., Clark, R., Baines, K.H., Jaumann, R., Nicholson, P.D., Kirk, R.L., Lopes, R., Lorenz, R.D., Mitchell, K., Wood, C.A., and the Cassini RADAR Team, 2007b. Near-infrared spectral mapping of Titan's mountains and channels. J. Geophys. Res. 112, doi:10.1029/2007JE002932. E11006.

Beyer, R.A., McEwen, A.S., Kirk, R.L., 2003. Meter-scale slopes of candidate MER landing sites from point photoclinometry. J. Geophys. Res. (Planets) 108, doi:10.1029/2007JE002120. 26-1.

Bourke, M.C., Balme, M., Beyer, R.A., Williams, K.K., Zimbelman, J., 2006. A comparison of methods used to estimate the height of sand dunes on Mars. Geomorphology 81, 440–452.

Brown, R.H., Baines, K.H., Bellucci, G., Bibring, J.-P., Buratti, B.J., Capaccioni, F., Cerroni, P., Clark, R.N., Coradini, A., Cruikshank, D.P., Drossart, P., Formisano, V., Jaumann, R., Langevin, Y., Matson, D.L., McCord, T.B., Mennella, V., Miller, E., Nelson, R.M., Nicholson, P.D., Sicardy, B., Sotin,

C., 2004. The Cassini Visual and Infrared Mapping Spectrometer (VIMS) investigation. Space Sci. Rev. 115, 111–168.

Brown, R.H., Griffith, C.A., Lunine, J.I., Barnes, J.W., 2006. Polar caps on Titan? In: European Planetary Science Congress, Berlin, Germany, September 18–22, 2006.

Buratti, B.J., Sotin, C., Brown, R.H., Hicks, M.D., Clark, R.N., Mosher, J.A., McCord, T.B., Jaumann, R., Baines, K.H., Nicholson, P.D., Momary, T., Simonelli, D.P., Sicardy, B., 2006. Titan: Preliminary results on surface properties and photometry from VIMS observations of the early flybys. Planet. Space Sci. 54, 1498–1509.

Burr, D.M., Carling, P.A., Beyer, R.A., Lancaster, N., 2004. Flood-formed dunes in Athabasca Valles, Mars: Morphology, modeling, and implications. Icarus 171, 68–83.

Herring, C., 1950. Effect of change of scale on sintering phenomena. J. Appl. Phys. 21, 301–303.

Hurford, T.A., Beyer, R.A., Schmidt, B., Preblich, B., Sarid, A.R., Greenberg, R., 2005. Flexure of Europa's lithosphere due to ridge-loading. Icarus 177, 380–396.

Jaumann, R., Brown, R.H., Stephan, K., Soderblom, L.A., Sotin, C., Le Mouèlic, S., Barnes, J.W., Clark, R.N., Buratti, B.J., Wagner, R., McCord, T.B., Rodriguez, S., Baines, K.H., Cruikshank, D.P., Nicholson, P.D., Griffith, C.A., 2008. Evidence for surface erosion by catastrophic runoff on Titan. Icarus, in press.

Lancaster, N., 1995. The Geomorphology of Desert Dunes. Routledge, London.

Le Mouèlic, S., Paillou, P., Janssen, M.A., Barnes, J.W., Rodriguez, S., Sotin, C., Brown, R.H., Baines, K.H., Buratti, B.J., Clark, R.N., Crapeau, M., Encrenaz, P.J., Jaumann, R., Geudtner, D., Paganelli, F., Soderblom, L., Tobie, G., Wall, S., 2007. Joint analysis of Cassini VIMS and RADAR data: Application to the mapping of Sinlap crater on Titan. J. Geophys. Res., doi: 10.1029/2007JE002965, in press.

Lorenz, R.D., Lunine, J.I., Grier, J.A., Fisher, M.A., 1995. Prediction of aeolian features on planets: Application to Titan paleoclimatology. J. Geophys. Res. 100, 26377–26386.

Lorenz, R.D., Wall, S., Radebaugh, J., Boubin, G., Reffet, E., Janssen, M., Stofan, E., Lopes, R., Kirk, R., Elachi, C., Lunine, J., Mitchell, K., Paganelli, F., Soderblom, L., Wood, C., Wye, L., Zebker, H., Anderson, Y., Ostro, S., Allison, M., Boehmer, R., Callahan, P., Encrenaz, P., Ori, G.G., Francescetti, G., Gim, Y., Hamilton, G., Hensley, S., Johnson, W., Kelleher, K., Muhleman, D., Picardi, G., Posa, F., Roth, L., Seu, R., Shaffer, S., Stiles, B., Vetrella, S., Flamini, E., West, R., 2006. The sand seas of Titan: Cassini RADAR observations of longitudinal dunes. Science 312, 724–727.

Lorenz, R.D., Clark, R., Curchin, J., Hoefen, T., 2008. Organic ices at cryogenic temperatures: First steps towards a 'Mohs scale' for Titan geological materials. Icarus, submitted for publication.

McCord, T.B., Hansen, G.B., Buratti, B.J., Clark, R.N., Cruikshank, D.P., D'Aversa, E., Griffith, C.A., Baines, E.K.H., Brown, R.H., Dalle Ore, C.M., Filacchione, G., Formisano, V., Hibbitts, C.A., Jaumann, R., Lunine, J.I., Nelson, R.M., Sotin, C., and the Cassini VIMS Team, 2006. Composition of Titan's surface from Cassini VIMS. Planet. Space Sci. 54, 1524–1539.

McCord, T.B., Hayne, P., Combe, J.-P., Hansen, G.B., Barnes, J.W., Rodriguez, S., Le Mouèlic, S., Baines, K.H., Brown, R.H., Buratti, B.J., Sotin, C., Nicholson, P., Jaumann, R., Nelson, R., 2008. Titan's surface: Search for spectral diversity and composition using the Cassini VIMS investigation. Icarus 194, 212–242.

Persi Del Marmo, P., Iess, L., Picardi, G., Seu, R., Bertotti, B., 2007. The determination of Titan's rotational state from Cassini SAR images. In: 39th Annual AAS Division of Planetary Sciences Meeting.

Press, W.H., Teukolsky, S.A., Vetterling, W.T., Flannery, B.P., 1992. Numerical Recipes in C. The Art of Scientific Computing. Cambridge University Press, Cambridge, UK.

Radebaugh, J., Lorenz, R.D., Kirk, R., Lunine, J., Lopes, R., Wall, S., Team, R., 2007. Mountains on Titan observed by Cassini RADAR. Icarus 192, 77–91.

Radebaugh, J., Lorenz, R.D., Lunine, J.I., Wall, S.D., Boubin, G., Reffet, E., Kirk, R.L., Lopes, R.M., Stofan, E.R., Soderblom, L., Allison, M., Janssen, M., Paillou, P., Callahan, P., Spencer, C., and the Cassini RADAR Team, 2008. Dunes on Titan observed by Cassini RADAR. Icarus, doi: 10.1016/j.icarus.2007.10.015, in press.

Rodriguez, S., Le Mouélic, S., Sotin, C., Clénet, H., Clark, R.N., Buratti, B., Brown, R.H., McCord, T.B., Nicholson, P.D., Baines, K.H., and the VIMS Science Team, 2006. Cassini/VIMS hyperspectral observations of the HUYGENS landing site on Titan. Planet. Space Sci. 54, 1510–1523.

Rubin, D.M., Ikeda, H., 1990. Flume experiments on the alignment of transverse, oblique, and longitudinal dunes in directionally varying flows. Sedimentology 37, 673–684.

Soderblom, L., Kirk, R.L., Lunine, J.I., Anderson, J.A., Baines, K.H., Barnes, J.W., Barrett, J.M., Brown, R.H., Buratti, B.J., Clark, R.N., Cruikshank, D.P., Elachi, C., Janssen, M.A., Jaumann, R., Karkoschka, E., Le Mouèlic, S., Lopes, R.M., Lorenz, R.D., McCord, T.B., Nicholson, P.D., Radebaugh, J., Rizk, B., Sotin, C., Stofan, E.R., Sulcharski, T.L., Tomasko, M.G., Wall, S.D., 2007. Correlations between Cassini VIMS spectra and RADAR SAR images: Implications for Titan's surface composition and the character of the huygens probe landing site. Planet. Space Sci. 55, 2025–2036.

Sotin, C., Jaumann, R., Buratti, B.J., Brown, R.H., Clark, R.N., Soderblom, L.A., Baines, K.H., Bellucci, G., Bibring, J.-P., Capaccioni, F., Cerroni, P., Combes, M., Coradini, A., Cruikshank, D.P., Drossart, P., Formisano, V., Langevin, Y., Matson, D.L., McCord, T.B., Nelson, R.M., Nicholson, P.D., Sicardy, B., Le Mouèlic, S., Rodriguez, S., Stephan, K., Scholz, C.K., 2005. Release of volatiles from a possible cryovolcano from near-infrared imaging of Titan. Nature 435, 786–789.

Stiles, B., Kirk, R., Lorenz, R., Hensley, S., Lee, E., Ostro, S., Gim, Y., Hamilton, G., Johnson, W.T., West, R.D., and the Cassini RADAR Team, 2007. Estimating Titan's spin state from Cassini SAR Data. In: 39th Annual AAS Division of Planetary Sciences Meeting.

Tomasko, M.G., Archinal, B., Becker, T., Bézard, B., Bushroe, M., Combes, M., Cook, D., Coustenis, A., de Bergh, C., Dafoe, L.E., Doose, L., Douté, S., Eibl, A., Engel, S., Gliem, F., Grieger, B., Holso, K., Howington-Kraus, E., Karkoschka, E., Keller, H.U., Kirk, R., Kramm, R., Küppers, M., Lanagan, P., Lellouch, E., Lemmon, M., Lunine, J., McFarlane, E., Moores, J., Prout, G.M., Rizk, B., Rosiek, M., Rueffer, P., Schröder, S.E., Schmitt, B., See, C., Smith, P., Soderblom, L., Thomas, N., West, R., 2005. Rain, winds and haze during the Huygens probe's descent to Titan's surface. Nature 438, 765–778.

Tsoar, H., 1983. Dynamic processes acting on a logitudinal (Seif) dune. Sedimentology 30, 567–578.

Waite, J.H., Young, D.T., Cravens, T.E., Coates, A.J., Crary, F.J., Magee, B., Westlake, J., 2007. The process of tholin formation in Titan's upper atmosphere. Science 316, 870–875.

Wasson, R.J., Fitchett, K., Mackey, B., Hyde, R., 1988. Large-scale patterns of dune type, spacing and orientation in the Australian continental dunefield. Aust. Geogr. 19, 89–104.

White, K., Goudie, A., Parker, A., Al-Farraj, A., 2001. Mapping the geochemistry of the northern Rub Al Khali using multispectral remote sensing techniques. Earth Surf. Proc. Land. 26 (7), 735–748.